

# Dynamic energy spectrum and energy deposition in solid target by intense pulsed ion beams

Xiao Yu<sup>1,2,3,4</sup> · Zheng Liu<sup>5</sup> · Jie Shen<sup>1,2,3</sup> · Yu I. Isakova<sup>6</sup> · Hao-Wen Zhong<sup>1,2,3</sup> · Jie Zhang<sup>1,2,3</sup> · Sha Yan<sup>7</sup> · Gao-Long Zhang<sup>1,2,3</sup> · Xiao-Fu Zhang<sup>1,2,3</sup> · Xiao-Yun Le<sup>1,2,3</sup>

Received: 20 June 2016/Revised: 25 July 2016/Accepted: 3 August 2016/Published online: 27 February 2017  
© Shanghai Institute of Applied Physics, Chinese Academy of Sciences, Chinese Nuclear Society, Science Press China and Springer Science+Business Media Singapore 2017

**Abstract** A method for analyzing the dynamic energy spectrum of intense pulsed ion beam (IPIB) was proposed. Its influence on beam energy deposition in metal target was studied with IPIB produced by two types of magnetically insulated diodes (MID). The emission of IPIB was described with space charge limitation model, and the dynamic energy spectrum was further analyzed with time-of-flight method. IPIBs generated by pulsed accelerators of BIPPAB-450 (active MID) and TEMP-4M (passive MID) were studied. The dynamic energy spectrum was used to deduce the power density distribution of IPIB in the target with Monte Carlo simulation and infrared imaging diagnostics. The effect on the

distribution and evolution of thermal field induced by the characteristics of IPIB dynamic energy spectrum was discussed.

**Keywords** Intense pulsed ion beam · Space charge · Time-of-flight method · Dynamic energy spectrum · Power density distribution

## 1 Introduction

Intense pulsed ion beams (IPIBs) originated as the candidate for ignition for inertial confined fusion have been extensively researched during the past three decades in materials science and engineering in the USA, Russia/USSR, Japan, etc. [1]. This technology has been used in applications of surface modification [2–4], nanopowder preparation, thin films deposition [5] and test of materials under high heat flux for nuclear fusion reactors [6], typically using IPIBs with energy density of several J/cm<sup>2</sup>. In IPIB irradiation of targets, by the short pulse duration of less than 1 μs and the ion range of several μm, the beam energy is highly compressed in time and space domain. Sharp temperature changes in the near-surface region of the target can be induced by the extremely high power density, leading to melting, vaporizing, ablation and ultra-fast resolidification [2] with shock waves being ignited by the thermal shock in the bulk of target [7]. The interaction mechanism between IPIB and the target, especially the thermal response, is vital to understanding the phenomenon in material modification. Due to difficulties experimental observation of the dynamic process of IPIB energy deposition and induced thermal field, researches in

---

This work is supported by the National Natural Science Foundation of China (No. 11175012) and the National Magnetic Confinement Fusion Program (No. 2013GB109004).

---

✉ Xiao-Yun Le  
xyle@buaa.edu.cn

- <sup>1</sup> School of Physics and Nuclear Energy Engineering, Beihang University, Beijing 100191, China
- <sup>2</sup> International Research Center for Nuclei and Particles in the Cosmos, Beihang University, Beijing 100191, China
- <sup>3</sup> Beijing Key Laboratory of Advanced Nuclear Materials and Physics, Beihang University, Beijing 100191, China
- <sup>4</sup> School of Space and Environment, Beihang University, Beijing 100191, China
- <sup>5</sup> Department of Mechanical Engineering, Tsinghua University, Beijing 100084, China
- <sup>6</sup> Institute of High Technology Physics, Tomsk Polytechnic University, Tomsk, Russia 634050
- <sup>7</sup> Institute of Heavy Ion Physics, Peking University, Beijing 100871, China

this field rely heavily on numerical simulation, in which the key issue is the energy deposition of IPIB as it renders the source term.

To describe the IPIB energy deposition in the targets, it is necessary to figure out the spatial and temporal distribution of the beam energy in the target. This requires to estimate the energy loss of ions in matter and how the count of ions changes. IPIBs are often regarded as mono-energetic [8] and deposited power of IPIB is calculated by fitting the accelerating voltage and the IPIB current density waveforms to a Gaussian shape, and then take their product [9, 10]. Drawbacks in these approximations are obvious: The diode voltage and beam current waveforms acquired by experiments are usually found dissimilar to Gaussian [7–11], and the ion current density curve may change during the beam transportation as it is not mono-energetic. All these question the energy balance of the models. In short, the spatial and temporal characteristics of the dynamics in beam emission and transportation are not fully considered. And in the time-of-flight (TOF) method proposed to describe the temporal distribution of the energy spectrum [11], the ratio of ions in different energies is not clearly demonstrated since the beam emission dynamics is not fully taken into consideration.

In this paper, the space charge effect in beam emission is taken into account and the beam current formed by protons and  $C^+$  ions is calculated from the working voltage of the magnetically insulated diode (MID). Two sets of experiments are carried out on MID in active and passive working modes. The dynamic energy spectra of IPIB are used to calculate the density function of energy distribution probability. Then the cross-sectional energy density, measured by infrared imaging diagnostics, is projected with this probability function to power density distribution in the target. The influence of IPIB power density distribution is checked by applying to thermal response simulation.

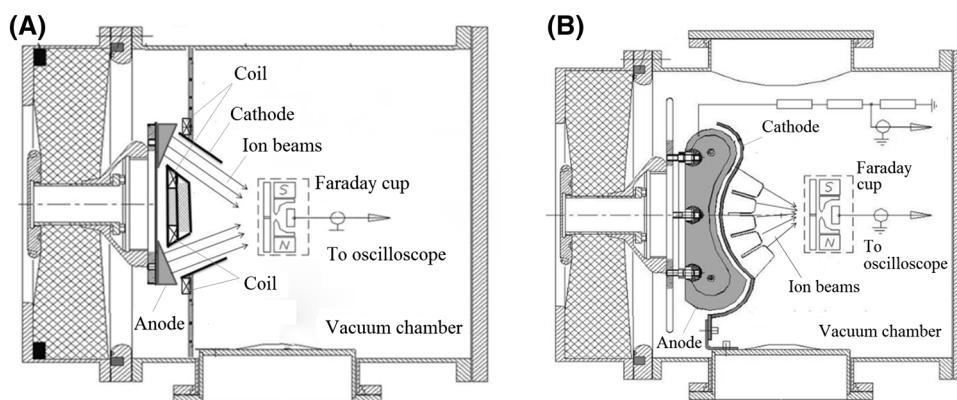
## 2 MID accelerators

In order to build the dynamic relation between the ion emission and IPIB energy spectrum, experiments were carried out on accelerators of BIPPAB-450 at Beihang University and TEMP-4M at Tomsk Polytechnic University, as shown in Fig. 1.

Technical details of the two MID accelerators can be found in Refs. [12, 13]. The basic working principle of an MID accelerator is as follows. Dense plasma is formed by high voltage pulses on the anode surface of MID. A transverse magnetic field is applied to the anode–cathode gap to deflect the electrons and prolong their moving trajectories. In this way, the electron flow in the plasma is suppressed and equivalently the ion flow is enhanced (i.e., magnetic insulation of the electron flow). The accelerated ions are extracted, ballistically focused to form IPIBs. IPIBs consist of protons and carbon ions. The IPIBs of BIPPAB-450, generated by flashover of polymers, are rich of protons, while the TEMP-4M IPIBs, formed by graphite explosive emission, are rich of carbon ions. The MID of BIPPAB-450 works under a single-pulse mode, while the MID in TEMP-4M is driven by a two-pulse mode with a pre-pulse to form the plasma. The magnetic field in the anode–cathode gap of BIPPAB-450 is generated by a pair of coaxial coils (active mode), while the magnetic field of TEMP-4M is formed by the construction of MID rather than powered windings (passive mode). The maximum value of working voltage is 450 kV for BIPPAB-450, while it is 250 kV for TEMP-4M.

IPIBs were generated by MID accelerators. The working voltage and beam current density were measured. A capacitive voltage divider was used to measure the diode voltage waveform. To overcome the Cullum repulsion of the positive charges and make stable transportation, IPIBs were neutralized with electrons. A Faraday cup with magnetic field [12, 13] was used to deflect the electrons and measure the ion beam current density.

**Fig. 1** Functional schematics of MID accelerators of **a** BIPPAB-450 and **b** TEMP-4M



### 3 Analysis and modeling method

#### 3.1 IPIB dynamic energy spectrum

It is assumed that protons and C<sup>+</sup> ions are formed simultaneously on the anode surface, the drift velocity of the ions does not vary in flight, the ion density of IPIBs in both MIDs is lower than 10<sup>12</sup> cm<sup>-3</sup>, and the scattering between ions is negligible.

Considering the space charge effect, the ion current density formed by a certain type of ions can be described by the Child–Langmuir law (i.e., the three-halves power law) under non-relativistic approximation:

$$J_{\text{ion}} = \frac{4K\epsilon_0\sqrt{2Z}}{9\sqrt{m}} \cdot \frac{U^{3/2}}{(d_0 - vt)^2}, \tag{1}$$

where  $U$  is the working voltage of the anode,  $d_0$  is the initial anode–cathode gap ( $d_0 = 7.5$  mm for BIPPAB-450 and  $d_0 = 8$  mm for TEMP-4M),  $\epsilon_0$  is the permittivity of vacuum,  $v$  is the diffusion velocity of the plasma on the MID anode surface,  $m$  is the ion mass,  $Z$  is the ion charge and  $K$  is the amplification constant for an ion species. In this way, the accelerating voltage (i.e., the ion energy) and IPIB emission are correlated.

The time of flight of the ions is given by Eq. (2) to calculate the current density after transportation:

$$\text{TOF} = D\sqrt{\frac{m}{2ZU}}, \tag{2}$$

where  $D$  is the anode–target distance ( $D = 20$  cm for BIPPAB-450 and  $D = 14$  cm for TEMP-4M).

The absolute value of the beam current density is calculated by fitting the calculated beam current density to the measured data by modulating the amplification coefficient  $K$  in Eq. (1). As the proton signal appears first due to its short TOF, the  $K$  of protons is fixed first, and then the  $K$  of carbon ions is fixed with the later part of the beam current.

#### 3.2 IPIB power density distribution function

Based on the IPIB dynamic energy spectrum above, Eq. (3) can be established to calculate the power density distribution of IPIB in the target: At time  $t$ , the energy loss of IPIB in the depth  $z$  in the target can be expressed as:

$$\begin{aligned} \left(\frac{dE}{dz}\right)_t &= N_1\left(\frac{dE}{dz}\right)_{1,H} + N_2\left(\frac{dE}{dz}\right)_{2,H} + N_3\left(\frac{dE}{dz}\right)_{3,C} \\ &+ N_4\left(\frac{dE}{dz}\right)_{4,C} + \dots, \end{aligned} \tag{3}$$

where  $(dE/dZ)_{i,V}$  is the energy loss of ion  $V$  (protons or C<sup>+</sup> ions) at time  $t$  and count  $N_i$ .

The total energy deposition of the ion beam is:

$$S(z, t) = \sum_j \left(\frac{dE}{dz}\right)_{t_j}. \tag{4}$$

Take  $S'(z, t)$  as the normalization of  $S(z, t)$ :

$$S'(z, t) = \frac{S(z, t)}{\iint S(z, t) dz dt}. \tag{5}$$

$S'(z, t)$  is the bidimensional probability density distribution. The power density distribution of IPIB can be written as:

$$P(x, y, z, t) = S'(z, t)Q(x, y), \tag{6}$$

where  $Q(x, y)$  has a dimension of energy per unit area, means the cross-sectional energy density of IPIB and can be measured by calorimeters or infrared imaging diagnostics [14, 15]. With  $S'(z, t)$ , the cross-sectional energy density of IPIB on the target is projected to the power density distribution in the target and the energy balance between the beam diagnostics and the source term of modeling is thus established. Another common method of approximation, the variable separation (VS) [13] is taken for comparison. In this method,  $S'(z, t)$  is expressed as:

$$S'(z, t) = d(z)g(t), \tag{7}$$

where  $d(z)$  is depth-normalized ion energy loss function (in this paper an energy-weighted average ion energy is used for the calculation) and  $g(t)$  is time-normalized beam power evolution function (here the normalization of the ion beam current density curves is used). The power density distribution is:

$$P(x, y, z, t) = S'(z, t)Q(x, y) = d(z)g(t)Q(x, y). \tag{8}$$

The energy loss of ions in 304 stainless steel is calculated with SRIM code [16]. A typical value of IPIB cross-sectional energy density,  $Q = 0.5$  J/cm<sup>2</sup> [13], is adopted for calculating  $P$ .

#### 3.3 IPIB thermal response simulation

Influence of IPIB power distribution is studied with thermal field simulation. Within 1 μs, as the lateral heat conduction is much weaker than that along the depth [17], one-dimensional approximation is adopted. The thermal response in the target is described by Fourier heat conduction equation:

$$\rho C_V \frac{\partial T}{\partial t} = \lambda \frac{\partial^2 T}{\partial z^2} + P, \tag{9}$$

where  $T(z, t)$  is the target temperature and  $\rho$ ,  $C_V$  and  $\lambda$  are density, specific heat and thermal conductivity of the target, respectively. For initial condition:

$$T(z, 0) = T_0 = 298 \text{ K.} \quad (10)$$

The radiative boundary condition is taken on the surfaces:

$$j = \varepsilon\sigma(T^4 - T_0^4), \quad (11)$$

where  $j$ ,  $\sigma$  and  $\varepsilon$  are the radiative heat flux, Stefan–Boltzmann constant and emissivity, respectively. For stainless steel,  $\varepsilon = 0.3$ . Equation (11) can be solved by finite element software COMSOL Multiphysics.

## 4 Results and discussion

### 4.1 Dynamic energy spectra of IPIB

As IPIB is formed by hydrogen-rich polymers in BIP-PAB-450, the proton component in the ion beam is much higher than carbon ions (Fig. 2Aa). The calculated proton and  $C^+$  ion current densities are of the loop-like shape. This can be explained as follows. The first emitted low energy ions with a longer TOF may arrive simultaneously at the Faraday cup, while the high energy ions are emitted by higher voltage and as depicted by the Child–Langmuir law, with larger counts, forming the branch of larger current density. The peaks in the current density can be well described, yet the rising edge of the current density curve cannot be well fitted, due to fluctuations in the diode voltage before the main accelerating pulse acts on the anode. Projected curves on the  $E$ – $J$  plane in Fig. 2Ab show

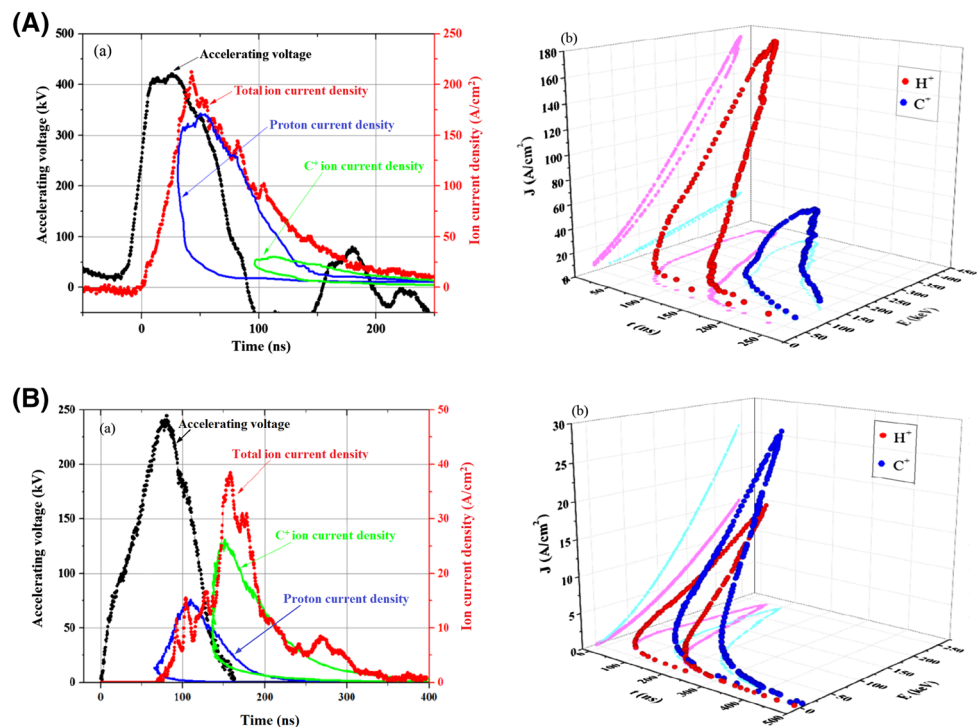
that the peak height of the IPIB current density is in correspondence with ions of the highest energy, which follows the Child–Langmuir law and differs notably from the mono-energetic and Gaussian approximation in previous studies [8–10]. At the beginning, the beam current consists mainly of protons due to the shorter TOF of protons. After 90 ns, the beam current pulse of  $C^+$  ions arrives at the target with much smaller count and a lower portion in energy deposition.

As shown in Fig. 2B, the carbon component of IPIB is dominant in TEMP-4M. A smaller peak of protons with lower count can be seen in the beam current, before the main peak of carbon ions with much higher count (Fig. 2Ba). The main trend of the temporal distribution of the beam current distribution comes with the prescription of the Child–Langmuir law, yet the fine structure of beam current, especially the small peaks in the proton beam current, cannot be well described. A possible reason is that the MID of TEMP-4M is first driven by a negative pulse to form the plasma on the anode surface, causing fluctuations in the emission of protons, a species easy to be perturbed due to its small ion mass.

### 4.2 Power density distribution of IPIB in the target

Due to the compression by short pulse duration and ion range, a peak of over  $10^{16} \text{ W/m}^3$  can be reached (Fig. 3) in the power density distribution. Several discrete peaks can be resolved by the TOF method (Fig. 3b) as the temporal

**Fig. 2** Data and analysis on (a) BIPPAB-450 and (b) TEMP-4M: *a* waveform of accelerating voltage by oscilloscope, total ion current density by Faraday cup and the calculated current density of  $H^+$  and  $C^+$  ions. *b* The calculated dynamic energy spectrum



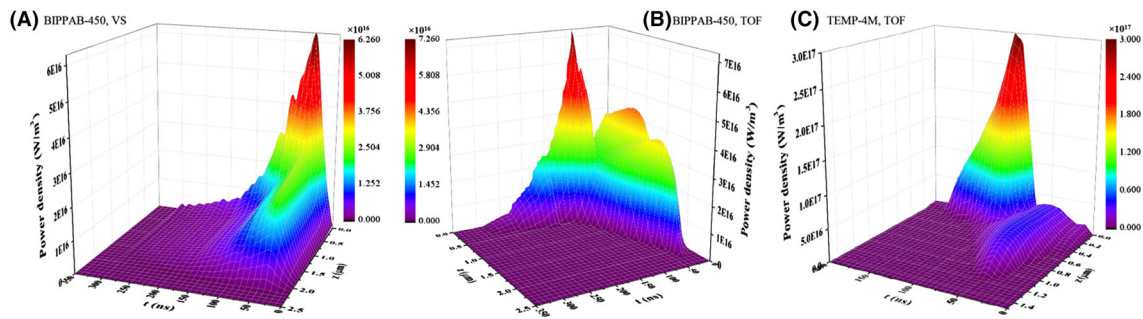


**Fig. 3** Power density distribution of  $0.5 \text{ J/cm}^2$  IPIB in 304 stainless steel target on BIPPAB-450 and TEMP-4M

sequence of the ion beam can be analyzed, while in the VS (variable separation) method (Fig. 3a) the distribution of beam energy displays a much smoother trend. For the IPIB produced by BIPPAB-450, in the first 100 ns, the energy deposition is governed by protons in a depth of up to  $2 \mu\text{m}$  and is characterized by two Bragg peaks formed by protons of different energies. After 100 ns, as the range of  $\text{C}^+$  ions is much shorter ( $<0.5 \mu\text{m}$ ), another high peak is formed. Due to the space charge effects, higher ion energy corresponds to larger ion count. A larger portion of the beam energy concentrates to the peaks in the TOF method than that in the VS method. Consequently, after 100 ns in a depth of  $>1 \mu\text{m}$ , the power density calculated by the TOF method is much lower than that obtained by the VS method due to the absence of protons.

In the first 70 ns of the IPIB of TEMP-4M, the energy deposition is dominated by protons. After that, as the carbon ions arrived with much larger counts much shorter ranges in the target, a sharp rise in the power density is induced in the target within a depth of  $0.2 \mu\text{m}$ , making tremendous amplitude in instantaneous power density of up to several  $10^{17} \text{ W/m}^3$ . Although in all the cases the cross-sectional energy density of IPIB is the same, considerable difference in the distribution of deposited power density can be caused as the dynamic energy spectrum of the beam changes.

### 4.3 Thermal field evolution induced by IPIB radiation

The effect of the IPIB dynamic spectrum is further reflected by the thermal field induced by different source terms. For the BIPPAB-450, the maximum value of the thermal field by the TOF method is over 100 K higher than that by the VS method (Fig. 4a, b). The temperature change rates are higher by the TOF method, as a result of more intensive concentration of beam energy to the peaks resolved in the method. The temperature change induced by the TEMP-4M IPIB (Fig. 5c) is much higher ( $>1400 \text{ K}$ ) than that by the BIPPAB-450. As the beam energy is more intensively concentrated to a shallower region by higher carbon percentage, larger rates of the temperature rise and decline appear on the target surface. This means that with more intensively compressed beam energy, the thermal shock effect caused by the TEMP-4M is much stronger.

The temperature difference between the TOF and VS methods for the BIPPAB-450 is demonstrated in Fig. 5a. In the region within the maximum ion range ( $z < 3 \mu\text{m}$ ), the temperature rise by TOF method is higher than that by VS method at the beginning of the beam irradiation. After 100 ns, as there is no energy deposition in the depth deeper than  $0.5 \mu\text{m}$  (the maximum  $\text{C}^+$  range of BIPPAB-450) in the TOF method, higher temperature rise is induced by the

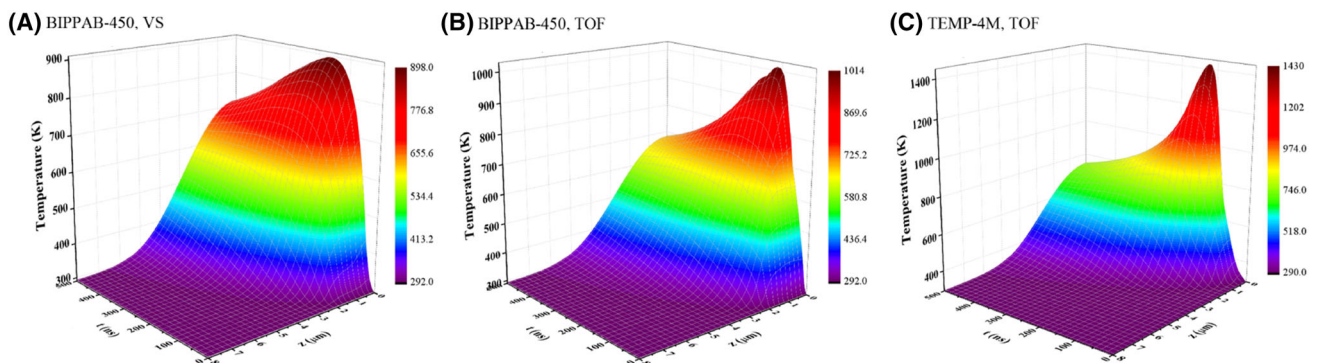


**Fig. 4** Thermal field induced by IPIB ( $0.5 \text{ J/cm}^2$ ) in 304 stainless steel on BIPPAB-450 and TEMP-4M

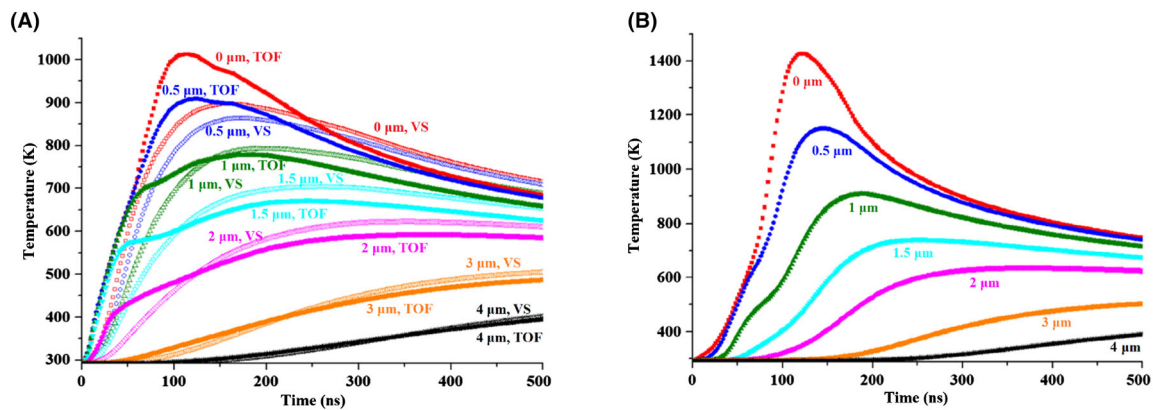


**Fig. 5** Temperature evolution at different depth by TOF and VS method on BIPPAB-450 (a) and by TOF method on TEMP-4M (b)

VS method as a result of direct energy deposition. In the region deeper than the ion range ( $4 \mu\text{m}$  in Fig. 5a), the temperature rise is induced by thermal conduction rather than beam energy deposition, and the trend in temperature evolution becomes similar for the two models.

For IPIB by TEMP-4M (Fig. 5b), within the ion range ( $z < 1 \mu\text{m}$ ), the maximum value and rising rate of the thermal field is higher than that of BIPPAB-450 as higher power density is deposited in this region. In the depth of  $1.5\text{--}2 \mu\text{m}$ , at the beginning of beam irradiation, the rising rate caused by BIPPAB-450 is higher as energy can be deposited in this position by long-range protons. After 200 ns, the temperature evolution becomes similar as the change in temperature is caused by heat conduction rather than beam energy deposition. In a depth of over  $4 \mu\text{m}$ , the temperature evolution, induced by heat conduction only, becomes similar for the two accelerators.

## 5 Conclusion

The dynamic energy spectrum is obtained by analyzing the IPIB emission under space charge limitation and transportation with the TOF method on both active and passive MIDs. The power density distribution of IPIBs is simulated with Monte Carlo method and cross-sectional energy diagnostics. The IPIB power density distribution acquired by TOF analysis is characterized by peaks formed by the temporal structure of the IPIB energy spectrum. Compared with the variable separation method, the beam energy is more highly concentrated to the peaks in the TOF method and induced higher thermal shock on the target surface.

The beam component has significant influence on the power density distribution. Ions with shorter range can make energy more intensively compressed to the shallower region in the target. Within the ion range, the power density distribution results in obvious variations in the thermal

field distribution and evolution. In the depth of over twice the ion range, changes in the thermal field are induced only by heat conduction and the trend of evolution becomes similar for different approximations.

**Acknowledgements** The authors appreciate Dr. G. E. Remnev, Dr. A. I. Pushkarev and Mr. I. P. Khailov of Tomsk Polytechnic University for their support in improving the experimental works.

## References

1. D.J. Rej, H.A. Davis, J.C. Olson et al., Materials processing with intense pulsed ion beams. *J. Vac. Sci. Technol. A* **1996**, 15 (1089). doi:10.1116/1.580435
2. G.E. Remnev, I.F. Isakov, M.S. Opekounov et al., High intensity pulsed ion beam sources and their industrial applications. *Surf. Coat. Technol.* **114**, 206 (1999). doi:10.1016/S0257-8972(99)00058-4
3. T.J. Renk, P.P. Provencio, S.V. Prasad et al., Materials modification using intense ion beams. *Proc. IEEE* **2004**, 92 (1057). doi:10.1109/JPROC.2004.829024
4. D.I. Proskurovsky, V.P. Rotshtein, G.E. Ozur et al., Physical foundations for surface treatment of materials with low energy, high current electron beams. *Surf. Coat. Technol.* **125**, 49 (2000). doi:10.1016/S0257-8972(99)00604-0
5. K. Yatsui, C. Grigoriu, K. Masugata et al., Preparation of thin films and nanosize powders by intense, pulsed ion beam evaporation. *Jpn. J. Appl. Phys.* **36**, 4928 (1997). doi:10.1143/JJAP.36.4928
6. J.A. Ruiz, A. Rivera, K. Mima et al., Plasma-wall interaction in laser inertial fusion reactors: novel proposals for radiation tests of first wall materials. *Plasma Phys. Contr. Fusion* **54**, 124051 (2012). doi:10.1088/0741-3335/54/12/124051
7. X. Le, S. Yan, Z. Liu et al., Detection of shocks generated by intense pulsed ion beam irradiation. *Surf. Coat. Technol.* **201**, 4991 (2007). doi:10.1016/j.surfcoat.2006.07.201
8. H. Akamatsu, M. Yatsuzuka, Simulation of surface temperature of metals irradiated by intense pulsed electron, ion and laser beams. *Surf. Coat. Technol.* **169**, 219 (2003). doi:10.1016/S0257-8972(03)00083-5
9. X. Le, S. Yan, W. Zhao et al., Computer simulation of thermal-mechanical effects of high intensity pulsed ion beams on a metal surface. *Surf. Coat. Technol.* **128**, 381–386 (2000). doi:10.1016/S0257-8972(00)00611-3

10. D. Wu, Y. Gong, J.Y. Liu et al., Model of intense pulsed ion beam and simulation study of energy deposited on target. *Surf. Coat. Technol.* **201**, 6573 (2007). doi:[10.1016/j.surfcoat.2006.09.079](https://doi.org/10.1016/j.surfcoat.2006.09.079)
11. J.P. Xin, X.P. Zhu, M.K. Lei, On time-of-flight ion energy deposition into a metal target by high-intensity pulsed ion beam generated in bipolar-pulse mode. *Surf. Coat. Technol.* **206**, 879 (2011). doi:[10.1016/j.surfcoat.2011.04.052](https://doi.org/10.1016/j.surfcoat.2011.04.052)
12. A.I. Pushkarev, Y.I. Isakova, A gigawatt power pulsed ion beam generator for industrial applications. *Surf. Coat. Technol.* **228**, 382 (2013). doi:[10.1016/j.surfcoat.2012.05.094](https://doi.org/10.1016/j.surfcoat.2012.05.094)
13. I. Yulia, Diagnostic equipment for the TEMP-4M generator of high-current pulsed ion beams. *J. Korean Phys. Soc.* **59**, 3531 (2011). doi:[10.3938/jkps.59.3531](https://doi.org/10.3938/jkps.59.3531)
14. X. Yu, J. Shen, M. Qu et al., Characterization and analysis of infrared imaging diagnostics for intense pulsed ion and electron beams. *Vacuum* **113**, 36 (2015). doi:[10.1016/j.vacuum.2014.12.003](https://doi.org/10.1016/j.vacuum.2014.12.003)
15. Y. Isakova. Infrared imaging diagnostics for parameters of powerful ion beams formed by a diode in a double-pulse mode, in *2011 IEEE Pulsed Power Conference*, Chicago, June 19–23, 2011
16. J.F. Ziegler, M.D. Ziegler, J.P. Biersack, SRIM—the stopping and range of ions in matter (2010). *Nucl. Instrum. Methods B* **2010**, 268 (1818). doi:[10.1016/j.nimb.2010.02.091](https://doi.org/10.1016/j.nimb.2010.02.091)
17. X. Yu, J. Shen, H. Zhong et al., Distribution and evolution of thermal field induced by intense pulsed ion beam on thin metal target. *Nucl. Instrum. Methods B* **365**, 225 (2015). doi:[10.1016/j.nimb.2015.07.061](https://doi.org/10.1016/j.nimb.2015.07.061)